UNIVERSITYOF BIRMINGHAM

Optical and electronic properties of mixed Ag-Au tetramer cations

Shayeghi, A.; Heard, C. J.; Johnston, R. L.; Schäfer, R.

Optical and electronic properties of mixed Ag-Au tetramer cations

A. Shayeghi, C. J. Heard, R. L. Johnston, and R. Schäfer

Articles you may be interested in

Copper doping of small gold cluster cations: Influence on geometric and electronic structure
J. Chem. Phys. **135**, 224305 (2011); 10.1063/1.3664307

Theoretical study of the electronic structure of M C H 2 + (M = Fe , Co , Ni)
J. Chem. Phys. **126**, 154318 (2007); 10.1063/1.2710259

Structure and spectral characteristics of the nanoalloy Ag 3 Au 10
Appl. Phys. Lett. **90**, 153123 (2007); 10.1063/1.2722702

Gas phase infrared spectroscopy of mono- and divanadium oxide cluster cations
J. Chem. Phys. **120**, 6461 (2004); 10.1063/1.1650833

Electronic structure of vanadium tetramer ion studied by optical absorption spectroscopy
J. Chem. Phys. **109**, 9737 (1998); 10.1063/1.477679

Optical and electronic properties of mixed Ag-Au tetramer cations

A. Shayeghi,[1,a)] C. J. Heard,[2] R. L. Johnston,[2] and R. Schäfer[1]

[1]*Eduard-Zintl-Institut, Technische Universität Darmstadt, Alarich-Weiss-Straße 8, 64287 Darmstadt, Germany*
[2]*School of Chemistry, University of Birmingham, Edgbaston, Birmingham B15 2TT, United Kingdom*

We present experimental and theoretical studies of the optical response of mixed $Ag_nAu_{4-n}^+$ (n=1–3) clusters in the photon energy range $\hbar\omega = 1.9$–3.5 eV. Absorption spectra are recorded by a newly built longitudinal molecular beam depletion spectroscopy apparatus providing lower limits to absolute photodissociation cross sections. The experimental data are compared to optical response calculations in the framework of long-range corrected time-dependent density functional theory with initial cluster geometries obtained by the unbiased Birmingham Cluster Genetic Algorithm coupled with density functional theory. Experiments and excited state calculations shed light on the structural and electronic properties of the mixed Ag-Au tetramer cations. © *2014 AIP Publishing LLC.*
[http://dx.doi.org/10.1063/1.4863443]

I. INTRODUCTION

A major goal of modern nanoscience is the study of size and composition-dependent physical and chemical properties of nanoscale materials with respect to their specific design and adaptation in advanced applications.[1,2] In particular, optical properties of nanoscale systems and building blocks are commonly investigated due to their importance in plasmonic sensing[3] and nanophotonics,[4] but also as a new class of nanoscale materials in general.[5]

The long term realization of such a goal, however, requires a fundamental investigation of the considered systems at the challenging atomic scale with model systems such as clusters containing only a few atoms. The noble metal elements gold and silver play a central role in current research particularly due to their very interesting optical properties.

While the optical properties of bare and rare gas tagged gold and silver clusters have been intensively investigated from both experimental[6–22] and theoretical points of view,[23–27] studies of their alloys at small sizes are rare at present, apart from photoelectron (PE) spectroscopy measurements of $Au_nAg_m^-$ ($2 \le n+m \le 4$) clusters.[28]

In general, less experimental information is available about small cationic Ag-Au clusters, except the ion mobility experiments of Weis *et al.*, who compared collision cross sections of $Ag_mAu_n^+$ ($m+n<6$) clusters to structural predictions from density functional theory (DFT).[29] They showed that most of the tetrameric clusters are rhombus shaped, while Ag_3Au^+ has a Y-structure with the gold atom in the center. They explained their results in terms of a significant charge transfer leaving most of the ions positive charge on the silver atoms. Bonačić-Koutecký *et al.* also discussed the dominant role of charge transfer from Ag to Au for structural properties in their investigation of neutral and charged bimetallic Ag_mAu_n ($3 \le m+n \le 5$) clusters.[30]

Gold, as a dopant, has a dominant influence on the optical properties of Ag clusters due to a strong relativistic effect,[31,32] leading to great interest in how the electronic behaviour of silver clusters for instance can be manipulated by doping them with gold.[33–36] From a theoretical point of view, optical properties of Ag-doped Au_{20} clusters have been studied by a first principles analysis showing the HOMO-LUMO transitions being shifted to lower photon energies with increasing Ag concentration.[37] Octameric Au_mAg_n ($m+n$=8) clusters have also been investigated using time-dependent density functional theory (TDDFT) showing odd–even oscillations of the optical gaps with the variation of the number of gold atoms.[38]

In this article, we present photodissociation spectra of $Ag_nAu_{4-n}^+$ (n=1–3) clusters in the photon energy range $\hbar\omega = 1.9$–3.5 eV combined with calculations of the optical response in the framework of TDDFT. Our initial cluster structures are obtained using the Birmingham Cluster Genetic Algorithm (BCGA),[39] coupled with DFT (GADFT).[40–44] The long-range corrected (LC) exchange correlation (xc) functional LC-ωPBEh, a version of LC-ωPBE,[45,46] with parameters recommended by Rohrdanz *et al.*,[47] is used in our analysis. It has been shown to perform well for the calculation of ground and excited state properties of gold,[27,48] and silver clusters,[48] where it leads to a reliable prediction of optical absorption spectra.

II. EXPERIMENTAL AND COMPUTATIONAL DETAILS

The experimental setup is described in detail in Ref. 48. Briefly, the tetramer cluster cations are produced by pulsed laser vaporization and separated by a time-of-flight mass spectrometer (TOF-MS). Before entering the acceleration zone of the TOF-MS and subsequent detection, the clusters are irradiated by a tunable ns-laser pulse in order to record photodissociation spectra by monitoring the ion signal depletion upon photon absorption. The Lambert–Beer law is used assuming a perfect overlap between dissociation laser and

a)Author to whom correspondence should be addressed. Electronic mail: shayeghi@cluster.pc.chemie.tu-darmstadt.de

molecular beam. Relative errors of our cross sections are estimated to be $\pm 10\%$ within the visible region and $\pm 30\%$ in the UV range as described in detail in our previous work. The experiment does not provide additional information about possible dissociation channels and therefore we cannot make any conclusions about the dynamics after photon absorption.

We employ an optical parametric oscillator (OPO) pumped by the third harmonic generation (355 nm) of an Nd:YAG laser extended with a harmonic generation unit as a tunable laser source to cover the photon energy range $\hbar\omega = 1.9$–3.5 eV. The available photon fluence is on average at least about $0.2/\text{Å}^2$ (356 nm) and at most about $0.5/\text{Å}^2$ (366 nm) in the UV range, while in the visible range it is at least $2.0/\text{Å}^2$ (410 nm) and at most $8.5/\text{Å}^2$ (562 nm).

Fluence dependencies of the main optical transitions of Ag_3Au^+ and $AgAu_3^+$ show an exponential decay and can be well-fitted with a single Lambert–Beer absorption law. Thus, the transitions can be attributed to one-photon processes. In the case of $Ag_2Au_2^+$ the situation is more complicated as the fluence dependencies cannot be fitted well with a single Lambert–Beer law and also not be described by a two-photon process, which argues for the simultaneous presence of several discrete isomers. However, a single Lambert–Beer absorption law does not rule out multiple species in the beam, if these species have similar absorption cross sections. But we would like to point out that, even in the case of a single isomer in the molecular beam, simultaneously occurring one- and two-photon processes could neither be interpreted with a multiple Lambert-Beer fit nor with a fit according to a two-photon process.

The configuration space for all tetramers is searched using the GADFT global optimization approach, in which the plane-wave self-consistent field (PWscf) code within the Quantum Espresso (QE) package,[49] has been coupled with the Lamarckian BCGA.[39] For the DFT calculations, 11 electrons for each atom are treated explicitly and the remaining 36 and 68 core electrons for Ag and Au, respectively, are described by ultrasoft Rabe-Rappe-Kaxiras-Joannopoulos pseudopotentials.[50] An additional nonlinear correction is applied for gold and the Perdew–Burke–Ernzerhof (PBE)[51] xc functional is employed within the generalized gradient approximation (GGA) framework of spin-unrestricted DFT. Within the code, local optimization of cluster structures is performed for each cluster in a generation, with an electronic self-consistency criterion of 10^{-5} eV, and total energy and force convergence considered to be reached when below the threshold values of 10^{-3} eV and 10^{-2} eV/Å, respectively.

The lowest lying potential global minimum (GM) candidates are subsequently locally optimized using NWChem v6.1,[52] employing an extensive 19-electron def2-TZVPP basis set and the corresponding effective core potential (def2-ECP) of Weigend and Ahlrichs.[53] The long-range corrected xc functional LC-ωPBEh[45,47] is used in order to accurately recover the asymptotic $1/r$ behaviour at large distances of the electrons from the nucleus. This has been shown to more reliably reproduce vertical electronic excitation spectra.[25,27,47,48,54] The PBE and the M06-L functional are also studied for comparison purposes. The energy is calculated using a grid of high density (*xfine* integration grid, *tight*

optimization criterion). Additionally, a harmonic frequency analysis is performed for all isomers in order to verify whether the structures are actually minima on the potential energy surface (PES).

Partial atomic valence charges are calculated for all DFT local minima at the LC-ωPBEh/def2-TZVPP level within the Bader approach using the program of Tang *et al.*[55] A cubic grid of $101 \times 101 \times 101$ points over a $5.0 \times 5.0 \times 5.0$ Å cube is used to calculate the Bader charges centred upon atomic sites.

For minimum-energy structures resulting from the DFT optimizations, electronic excitation spectra are calculated using spin-unrestricted TDDFT considering 60 excited states. All excited state calculations are performed with NWChem v6.1,[52] using the same xc functional and basis set as used in the geometry optimization step. The output from optical response calculations is analysed using Chemissian, an analytical tool for electronic structure and spectra calculations.[56]

An additional method for the structure elucidation of clusters is to perform ion mobility measurements. The experimental mobilities may be compared with calculated values for the set of candidate structures, as was utilized by Weis *et al.* to determine the structures of $Ag_mAu_n^+$ ($m+n<6$) considering the projection approximation (PA) and a modified trajectory method (TR).[29] For their trajectory calculations, Weis *et al.*[29] consider two situations, one in which the charge on the cluster is equally distributed (EQ-TR), and one in which the silver atoms equally transfer charge to the gold, for a total transfer of 0.5 *e* from Ag to Au.

PA corresponds to a simplification of the average collision cross section $\Omega_{avg}^{(1,1)}$, in which the projection of the possible contact area by He buffer gas travelling in the x direction upon the cluster is given as its shadow in the yz plane. Equation (1) shows the average collision cross section as an integral over the impact parameter b (which is a function of the scattering angle χ) and the relative velocities of gas and cluster v, then orientationally averaged over the three angles θ, ϕ, and γ, while μ is the reduced mass[57]

$$\Omega_{avg}^{(1,1)} = \frac{1}{8\pi^2} \int_0^{2\pi} d\theta \int_0^{\pi} d\phi \sin\phi \int_0^{2\pi} d\gamma \frac{\pi}{8} \left(\frac{\mu}{k_B T} \right)^3$$
$$\times \int_0^{\infty} db \, 2b(1 - \cos\chi(\theta, \phi, \gamma, v, b))$$
$$\times \int_0^{\infty} dv \exp(-\mu v^2/(2k_B T))v^5. \quad (1)$$

By counting the collision probability M/N upon this yz plane, for a set of N He atoms, the simplified cross section Ω is computed as Eq. (2). This model assumes hard spheres for both interaction species, and does not consider the effects of the anisotropy of the cluster, any local coordination effects or the interaction between the He gas and the charges on the cluster

$$\Omega = \frac{1}{4\pi} \int_0^{\pi} d\phi \sin\phi$$
$$\times \int_0^{2\pi} d\gamma \int_{-\infty}^{+\infty} \int_{-\infty}^{+\infty} M(\phi, \gamma, y, z) dy dz. \quad (2)$$

TR calculates the cross sections from a set of classical trajectories of the He gas over a set of collision events with the cluster. This requires an empirical potential V for He-cluster interactions of the Lennard Jones (LJ) + dipolar form of Eq. (3), where ε and σ are standard LJ parameters, α_{He} is the polarizability of helium, q_i is the charge on atom i of the cluster ion, and r_{ij} is the relative position of atom i in the j direction,

$$V = U_{LJ} + U_{Dipole}, \tag{3}$$

where

$$U_{LJ} = 4\varepsilon \sum_{i}^{n} \left[\left(\frac{\sigma_i}{r_i} \right)^{12} - \left(\frac{\sigma_i}{r_i} \right)^{6} \right] \tag{4}$$

and

$$U_{Dipole} = -\frac{\alpha_{He}}{8\pi\varepsilon_0} \sum_{j}^{3} \left(\sum_{i}^{n} \frac{q_i r_{ij}}{r_i^3} \right)^2. \tag{5}$$

In this work, we define a modified charge transfer trajectory calculation (CT-TR) method which uses the accurate Bader charges in order to further elucidate the structures and compare with previous results. For the low-lying minima of Ag-Au tetramer cations, calculated with the LC-ωPBEh functional, collision cross sections are calculated by the PA and the CT-TR method within the MOBCAL code of Mesleh et al.,[58] using the same potential parameters as Weis et al.:[29] $\varepsilon = 1.35$ meV, $\sigma_{AuHe} = 3.1$ Å, $\sigma_{AgHe} = 3.0$ Å, $r_{HardSphere} = 2.70$ Å and 2.63 Å for Au-He and Ag-He, respectively, and $\alpha_{He} = 0.205$ Å^3. For each TR simulation 2×10^6 classical trajectories are run.

III. RESULTS AND DISCUSSION

A. Calculated structures

Low energy isomers are obtained by the BCGA with the PBE functional, and subsequently locally optimized using a range of xc functionals frequently used for Au clusters: PBE, M06-L, and LC-ωPBEh at the LCAO-TZVPP level. M06-L is a local meta-GGA functional recommended for transition metal systems and those which exhibit non-covalent interactions.[59] LC-ωPBEh is a modified version of the range separated LC-ωPBE xc functional, which reproduces the long range asymptotic decay of the coulomb interaction by separating Hartree-Fock energies into long range and short range contributions. In our experience, the resulting structures and energies are very similar to those produced with LC-ωPBE, nevertheless we will restrict our analysis of theoretical absorption spectra to results obtained by LC-ωPBEh as will be shown in Sec. III B.

Figures 1–3 depict the energies of the four most stable structures produced with the BCGA locally optimized with all three functionals. The overlaid structures are those calculated with LC-ωPBEh, but all functionals give the same local minima, with minute distortions of bond lengths. The small size of the clusters ensures the BCGA is able to find every possible structure and permutational isomer (homotop) for each
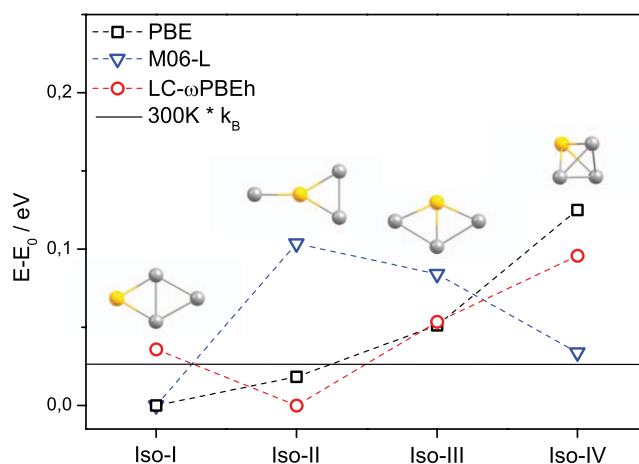

FIG. 1. Lowest lying Ag$_3$Au$^+$ isomers relaxed at the LC-ωPBEh/def2-TZVPP level of theory and their relative energies in eV (circles) compared to relative energies by the PBE (squares) and the M06-L (triangles) xc functional. Dashed lines connecting the data points are a guide to the eye. The horizontal line represents the thermal energy at 300 K. The LC-ωPBEh functional clearly determines the Y-shape isomer as the GM, contrary to the ordering predicted by the PBE and the M06-L functional.

composition. We have checked that no other isomers are introduced on local relaxations with different functionals.

Overall, we observe that there are three competing motifs, the rhombus, the distorted tetrahedron, and the Y-shaped structure, the last of which may exist in a symmetric or bent arrangement, depending on the composition and homotop.

The results of the PBE calculations are in almost perfect agreement with the findings of Weis et al.[29] (who used the BP86 functional) for all compositions, the only deviation is a reordering of the almost degenerate tetrahedron and bent Y-shape isomers of Ag$_2$Au$_2^+$ at 0.1 eV.

For Ag$_3$Au$^+$, there are four isomers from three structural motifs within 0.15 eV of the GM, for all functionals, suggesting a close competition for favourability in experiment. PBE and M06-L agree upon the rhombus-shaped Iso-I as the GM, whereas LC-ωPBEh suggests an additional stabilization of the Y-shaped cluster. Weis et al. claim that despite the slight

FIG. 2. Lowest lying Ag$_2$Au$_2^+$ isomers relaxed at the LC-ωPBEh/def2-TZVPP level of theory. For a description of symbols refer to Fig. 1. For the LC-ωPBEh functional, all isomers lie below 300 K in disagreement with qualitatively similar results obtained by the PBE and the M06-L functional, which only disagree in the description of the compact structure Iso-III.
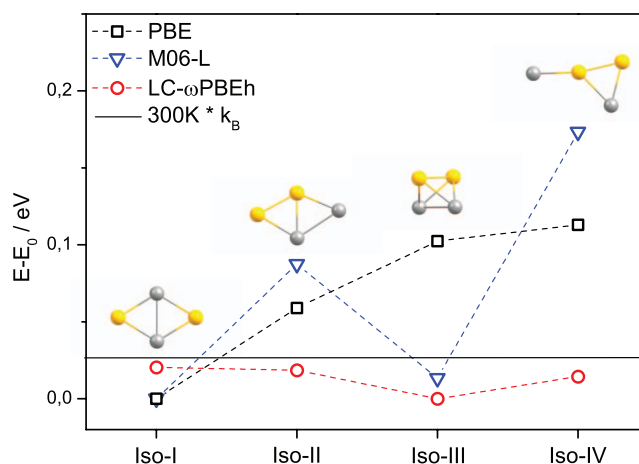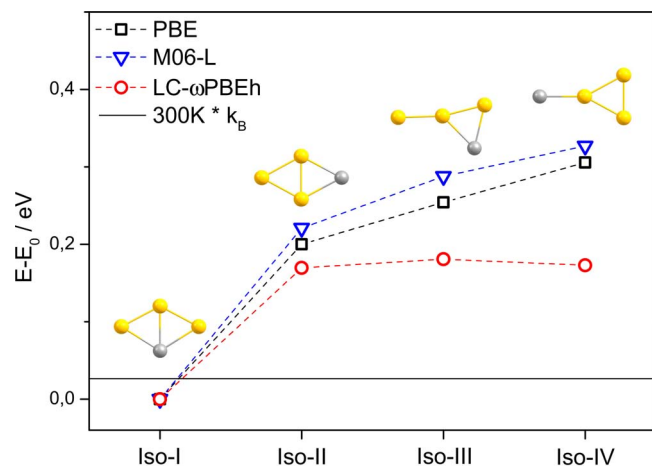
FIG. 3. Lowest lying $AgAu_3^+$ isomers relaxed at the LC-ωPBEh/def2-TZVPP level of theory. For a description of symbols refer to Fig. 1. In a qualitatively good agreement, all employed functionals find Iso-I being the most favored structural motif. For the LC-ωPBEh functional again the Y-shaped isomers seem to be generally more favored compared to the PBE and the M06-L functional which show similar results.

energetic preference for the rhombus (at the PBE level), the Y-shape is found in experiment, for which they cite the evidence of ion mobility collision cross section calculations for the Y-shape which fit the experimental data better than the rhombus.[29] Our LC-ωPBEh result supports this conclusion.

Overall, the range separated and PBE functionals agree well, whereas M06-L drastically favours the tetrahedron, and disfavours the Y-shaped structures, giving clear preference to maximal coordination.

For $Ag_2Au_2^+$, the two PBE-based functionals agree less well than for Ag_3Au^+ showing the strong influence of the LC in this case. While again, the lowest four isomers are identical, LC-ωPBEh suggests a narrowing of the energy spacings between minima, even to below the thermal energy at 300 K (shown as a horizontal solid line on each plot). This suggests that the rhombus, tetrahedron, and Y-shape can all potentially exist in the molecular beam, and while no thermal barriers are calculated, rearrangements between isomers may occur. Again, M06-L follows the trend of preference for higher coordination, with the Y-shape least favourable.

$AgAu_3^+$ displays excellent quantitative agreement between all three functionals, for which the rhombus is clearly preferred over the Y-shape, by a margin of around 0.2 eV, and thus experimentally we may expect the dominance of one isomer in the molecular beam. However, as in the case of $Ag_2Au_2^+$, LC-ωPBEh predicts a smaller energy difference between isomers than the other functionals. It is well established that gold clusters prefer planar structures up to a larger size than silver, with gold clusters reported to be planar for up to 7 atoms for the monocation.[60–62] But still it is surprising that even with the M06-L functional, the tetrahedral geometry has not been found at this level of theory in the lowest few isomers although it has been found for Au_4^+.[29,48]

The preference for a given structure is complicated to understand in the case of mixed clusters due to the presence of permutational isomers, the number of which depend on the symmetry of the cluster. For the Y-shape motif there are

up to four homotops for $Ag_2Au_2^+$, and the preference for a particular homotop depends sensitively on a number of factors, including homo- and heterophilicity, electronegativity, and atomic radius. It may be said that there is a first order preference, based on the result of these factors, in which atoms occupy sites on the rigid cluster, followed by a second order effect, which is the extra stabilization (or destabilization) of that isomer due to the structure itself, such as frustration for spin or charge distributions. In this way we may rationalize the preferred permutational isomers of the clusters investigated here.

For the tetrahedron, no conclusions may be drawn, as for a monodoped and 50:50 composition clusters, all sites and combinations are essentially degenerate. For the rhombus, we observe that silver atoms preferentially occupy the high coordination sites – most strikingly in the case of $AgAu_3^+$, which exhibits a large energy gap between the lowest isomers. This behaviour is commonly observed in mixed metal clusters containing gold,[35,63] and agrees exactly with the results of Bonačić-Koutecký, in which they claim heterometallic bonding is generally preferred,[30] and from which the only deviation is observed for Ag_3Au^+, which has nearly degenerate rhombic homotops. For $AgAu_3^+$, the rhombus containing three heterometallic bonds is preferred to the isomers with two, and in $Ag_2Au_2^+$, the homotop with four mixed bonds is preferable to that with three. This result is attributed to the maximization of charge-transfer from silver to gold, which is displayed in Table I.

For the Y-shaped clusters the trend of maximal Ag-Au mixed bonding no longer applies. We attribute this to the fact that the cluster has a frustrated geometry, with energetics dominated by charge transfer effects. Gold has a Pauling electronegativity of 2.5, as compared to 1.9 for silver, and draws significant charge from silver atoms. This may be seen most clearly for $AgAu_3^+$, in which the two-coordinate silver homotop is preferred to the three-coordinate, which in turn is higher

TABLE I. Site by site charge transfer of the four lowest lying isomers at the LC-ωPBEh level relative to +0.25 e/atom. Silver atoms are displayed in **bold**.

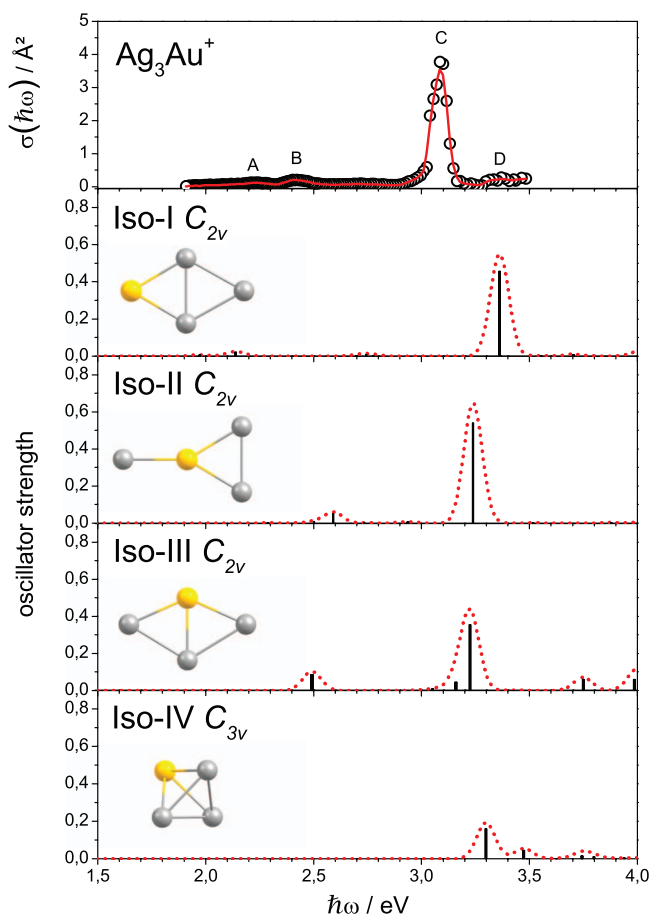|	Charge transfer e/atom		
	Ag_3Au^+	$Ag_2Au_2^+$	$AgAu_3^+$
Iso-I	**0.05**	−0.19	−0.11
	0.10	**0.19**	−0.03
	0.10	**0.19**	**0.25**
	−0.25	−0.19	−0.11
Iso-II	**0.13**	−0.17	**0.18**
	0.13	**0.21**	−0.04
	−0.42	−0.18	−0.10
	0.16	**0.14**	−0.04
Iso-III	**0.06**	−0.26	−0.12
	−0.28	−0.26	**0.26**
	0.06	**0.26**	−0.19
	0.16	**0.26**	0.05
Iso-IV	−0.39	−0.15	−0.01
	0.13	**0.25**	−0.21
	0.13	−0.30	**0.23**
	0.13	**0.20**	−0.01

FIG. 4. Experimental Ag_3Au^+ absorption spectrum data points (open circles) and a 3-pt adjacent average of these to guide the eye (solid line) compared to TDDFT calculations for the lowest lying isomers relaxed at the LC-ωPBEh/def2-TZVPP level of theory. The calculated linespectra (vertical lines) are convoluted with Gaussian functions with a full width at half maximum of 0.1 eV (dotted lines).

in energy even than the one-coordinated site. This result is explained by the frustrated nature of the Y-shape and is an example of a second order charge transfer effect. By comparison with the monometallic Ag_4^+ and Au_4^+ structures, we may decouple the effect due to the choice of homotop, and that from the structure itself. For rhombic Ag_4^+ and Au_4^+, there is negligible charge redistribution, beyond the $+0.25$ e/atom due to the single positive charge on the cluster. However, for the Y-shape, there is an additional accumulation of approximately 0.1 e/atom upon the central, three-coordinate site. This causes the gold atom to occupy this site. We therefore note that it is important to consider both causes of charge transfer when discussing the factors which determine homotop ordering in mixed metal clusters.

This charge transfer is maximized by gold occupation of the central site, and is a strong enough effect to outweigh the usual preference for low coordination.

B. Experimental and theoretical optical absorption spectra

1. Ag_3Au^+

Figure 4 shows the experimental absorption spectrum of Ag_3Au^+ in the photon energy range $\hbar\omega = 1.9$–3.5 eV

TABLE II. Oscillator strengths f of experimentally observed transitions (A–D) of the tetramers. Peak positions in eV as maxima of Gaussian fits to experimentally observed transitions are given in brackets.

	Oscillator strength f^a of transition			
Tetramers	A	B	C	D
Ag_3Au^+	0.015 (2.21)	0.018 (2.43)	0.334 (3.09)	…
$Ag_2Au_2^+$	0.078 (3.12)	…	…	…
$AgAu_3^+$	0.003(2.16)	0.012 (2.84)	0.195 (3.10)	0.037(3.28)

^{a}Determined by Gaussian deconvolution according to $f = 0.91103 \int_{Band} \sigma(\hbar\omega) d(\hbar\omega)$.[64]

and theoretical optical absorption spectra for the four lowest energy GADFT candidates from LC-TDDFT calculations. The experimental spectrum exhibits two smaller features at 2.21 eV (A) and 2.43 eV (B), and is dominated by an intense absorption at 3.09 eV (C) followed by a broad structure in the range 3.2–3.4 eV (D).

The comparison to TDDFT at the LC-ωPBEh/def2-TZVPP level of theory for the lowest lying isomers is shown below. The simulated spectra for Iso-I and Iso-IV can be ruled out, whereas Iso-II and Iso-III show a close competition in describing the experimental spectrum, capturing peaks B and C (also feature A for Iso-II with a very small oscillator strength of 0.008) with reasonable agreement on both position and relative oscillator strength.

Experimental oscillator strengths are calculated by Gaussian deconvolution of the respective peaks in an experimental spectrum. The values are given in Table II for all major peaks of each isomer. We find that for the intense transition C, values calculated with LC-ωPBEh for Iso-II (0.540) and Iso-III (0.399 as sum of oscillator strengths of two transitions in the range 3.1–3.3 eV), Iso-III gives a better agreement with the experimental value of 0.334. In addition, the slight tailing of signal C towards lower photon energies in the experimental spectrum seems to be better captured by Iso-III. However, it should be noted that the disagreement between theoretical
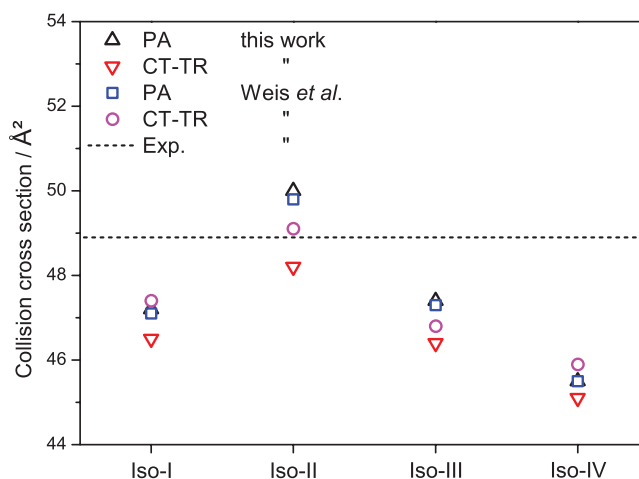

FIG. 5. Experimental collision cross section of Ag_3Au^+ (dashed line) compared to calculated collision cross sections for the lowest lying isomers obtained by the PA (squares) and the CT-TR (circles) approach (experiments and calculations taken from Ref. 29) and calculations for cluster geometries from this work also using the PA (triangles) and CT-TR (inverse triangles) approach including Bader charges in the CT-TR calculations.
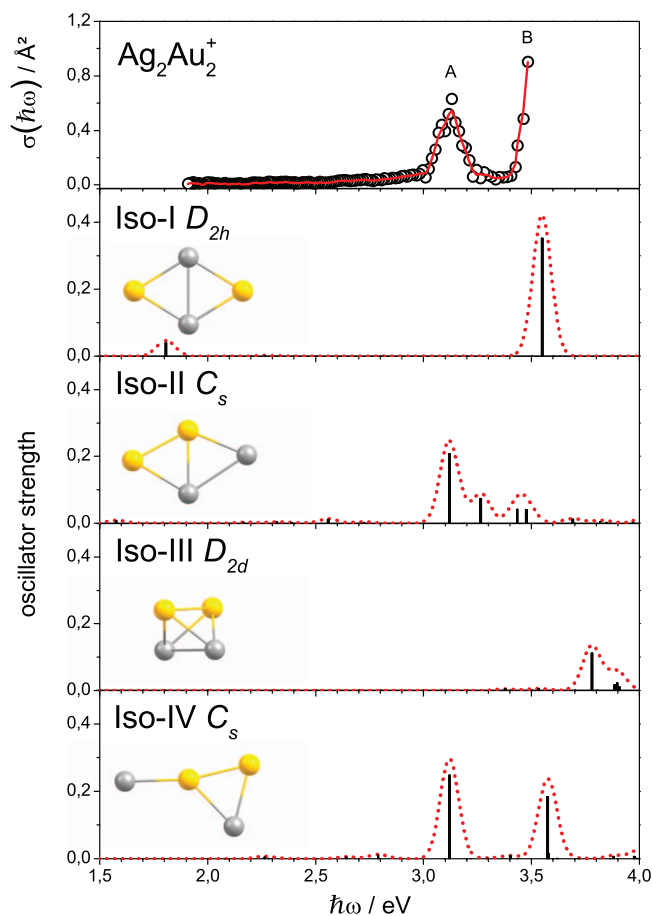
FIG. 6. Experimental $Ag_2Au_2^+$ absorption spectrum data points (open circles) and a 3-pt adjacent average of these to guide the eye (solid line) compared to TDDFT calculations for the lowest lying isomers relaxed at the LC-ωPBEh/def2-TZVPP level of theory. The calculated linespectra (vertical lines) are convoluted with Gaussian functions with a full width at half maximum of 0.1 eV (dotted lines).

and experimental oscillator strengths in general may either be attributed to inaccuracies of TDDFT or to experimental errors in measuring photodissociation cross sections. Hence, the comparison of oscillator strengths is not a sufficient criterion to rule out isomers especially in this case. Therefore, it is reasonable to compare the optical absorption spectra to ion mobility data in order to explicitly rule out one isomer.

In agreement with previous ion mobility experiments,[29] our calculated collision cross sections show the Y-shape with C_{2v} symmetry (Iso-II) to fit most closely with experimental data for both the PA and modified CT-TR methods (see Figure 5). This result is consistent with both the energetic analysis of the GADFT at the LC-ωPBEh level (see Figure 1) and the conclusions of the optical spectra simulations. It is clear that when Bader charges are included in the CT-TR approach, we may conclude unambiguously that Iso-II is the predominant species in the molecular beam.

2. $Ag_2Au_2^+$

Figure 6 shows the experimental absorption spectrum of $Ag_2Au_2^+$ and theoretical optical absorption spectra for the four lowest energy GADFT candidates from LC-TDDFT
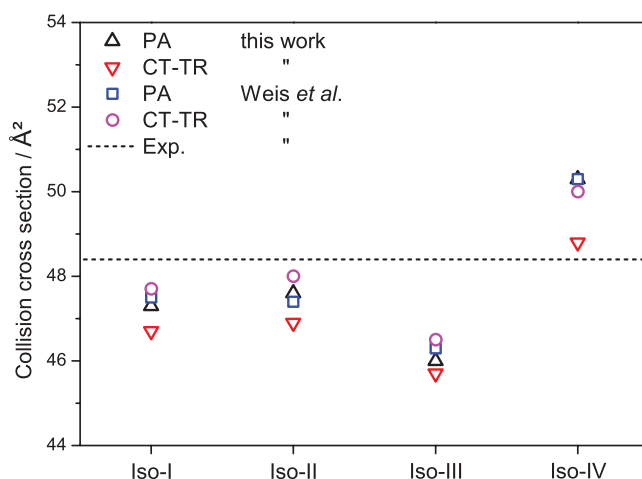

FIG. 7. Experimental collision cross section of $Ag_2Au_2^+$ (dashed line) compared to calculated collision cross sections for the lowest lying isomers obtained by the PA (squares) and the CT-TR (circles) approach (experiments and calculations taken from Ref. 29) and calculations for cluster geometries from this work also using the PA (triangles) and CT-TR (inverse triangles) approach including Bader charges in the CT-TR calculations.

calculations. The experimental spectrum shows a feature at 3.12 eV (A) and one transition with a maximum beyond the experimental range (B).

The comparison to the simulated optical response using LC-ωPBEh for the lowest lying isomers is presented below and shows a strong competition between isomers. In agreement with relative energies from LC-ωPBEh relaxations (see Fig. 2), the four lowest lying isomers are very close in energy and possibly all together present in the molecular beam. Even though the Y-shaped Iso-IV with C_s symmetry would be sufficient to qualitatively describe the experimental features A and B, the experimental oscillator strength of transition A (0.078) and the features of the spectrum could be explained by the sum of contributions from Iso-I and Iso-II. However, also Iso-IV or even a mixture of all three isomers could be present in the molecular beam (for experimental oscillator strengths see Table II).

The cluster with 1:1 composition presents a difficult situation for unambiguous structure elucidation, as there is a near energetic degeneracy of isomers in the GADFT predictions. Weis *et al.*[29] also note that the energetic separation between isomers is small, and the collision cross sections of each are very similar, and so do not claim to determine which structure is in existence. With the addition of our spectral predictions, we take the further step of claiming that several isomers are likely coexistent in the beam. As shown in Figure 7, the collision cross section of Iso-III is significantly lower than the experimental value, and this, coupled with its optical spectrum means we may tentatively exclude it. The systematic reduction of the CT-TR values we observe with our structures and charge method bring Iso-IV most in line with the experimental result, our mobility calculations indicate Iso-I and Iso-II move further from the experimental value, while iso-IV gets closer. But due to the close competition between isomer energies, it is unlikely that Iso-IV will be present in isolation in the molecular beam although it cannot be definitely ruled out.
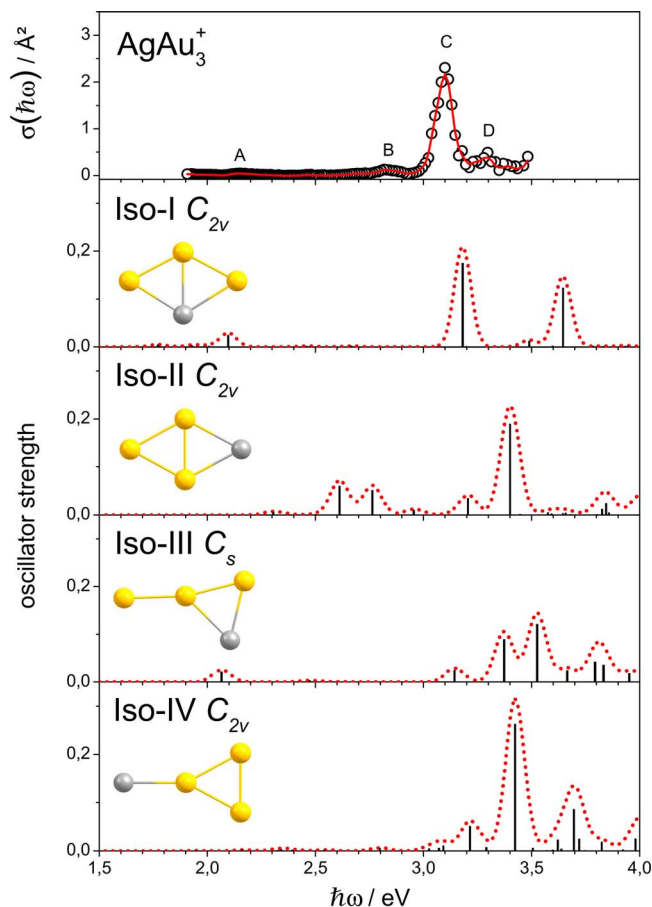
FIG. 8. Experimental AgAu$_3^+$ absorption spectrum data points (open circles) and a 3-pt adjacent average of these to guide the eye (solid line) compared to TDDFT calculations for the lowest lying isomers relaxed at the LC-ωPBEh/def2-TZVPP level of theory. The calculated linespectra (vertical lines) are convoluted with Gaussian functions with a full width at half maximum of 0.1 eV (dotted lines).

3. AgAu$_3^+$

Figure 8 shows the experimental absorption spectrum of AgAu$_3^+$ and theoretical optical absorption spectra for the four lowest energy GADFT candidates. The experimental spectrum shows two smaller features at 2.16 eV (A) and 2.84 eV (B), but is dominated by an intense absorption at 3.10 eV (C). The spectrum shows a broad weak feature at 3.28 eV (D) and a transition out of the experimental range at higher photon energies.

It is clear that the LC-TDDFT for Iso-I shows the best agreement with the experimental spectrum and agrees with the energy ordering of the GADFT results, for which Iso-I is the GM. Nevertheless, the experimental feature B is not covered by the calculated optical response for Iso-I and may potentially only be associated with a very weak transition at 2.67 eV with an oscillator strength of 0.002, which is hardly visible in Figure 8. However, its origin could also be attributed to a contribution of Iso-II to the experimental spectrum. But then one would expect more features to appear in the range 2.5–3.0 eV.

The oscillator strength for the intense experimental transition C (0.195) is in a very good agreement with the theoret-
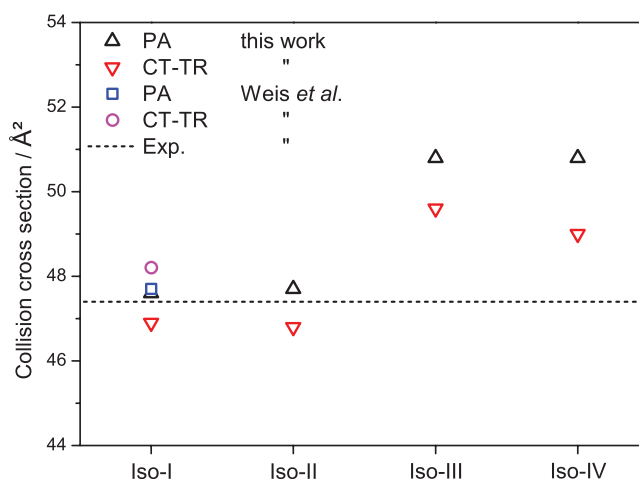

FIG. 9. Experimental collision cross section of AgAu$_3^+$ (dashed line) compared to calculated collision cross sections for the lowest lying isomers obtained by the PA (squares) and the CT-TR (circles) approach (experiments and calculations taken from Ref. 29) and calculations for cluster geometries from this work also using the PA (triangles) and CT-TR (inverse triangles) approach including Bader charges in the CT-TR calculations.

ical value (0.174) for the corresponding feature in the optical response of Iso-I at the LC-ωPBEh/def2-TZVPP level of theory (for experimental oscillator strengths see Table II).

It is clear from both spectral and GADFT analysis that there is likely only the one isomer, Iso-I in the molecular beam. Since the next isomer (Iso-II) is much higher in energy (0.17 eV at the LC-ωPBEh/def2-TZVPP level, see Figure 3), collision cross sections for AgAu$_3^+$ are only given for Iso-I in Ref. 29. For completeness we have calculated collision cross sections for the four lowest lying isomers (see Figure 9). It is unsurprising that Iso-III and Iso-IV exhibit cross sections vastly different from the experimental value, but interesting that Iso-II shows excellent agreement, essentially identical to Iso-I, because both Iso-I and Iso-II are rhombic structures, with very similar shapes. This underlies the importance of a multi-component analysis for structure elucidation. However, due to the large energetic discrepancy and the optical absorption spectra compared to TDDFT predictions, we conclude that only Iso-I is present in the experimental beam.

IV. CONCLUSIONS

The measured photodissociation spectra presented here have been shown to be useful for determining the structures of the Ag-Au tetramer cations in the molecular beam, when combined with systematic structural minima search and subsequent LC-TDDFT calculations. Our investigations from both experimental and theoretical points of view are in good agreement with previous ion mobility measurements, not only supporting their validity, but also allowing a different perspective on the electronic properties of the systems considered here. In general, the methods used allow an extensive correlation to be made between experimental data and electronic structure analysis.

While in the case of Ag$_3$Au$^+$ and AgAu$_3^+$ the Y-shaped Iso-II (C_{2v}) and the rhombus Iso-I (C_{2v}), respectively, can be clearly assigned, the situation is complicated in the case

of $Ag_2Au_2^+$. The nearly degenerate isomers (at the LC-ωPBEh/def2-TZVPP level of theory) Iso-I (D_{2h}), Iso-II (C_s), and Iso-IV (C_s) can all potentially contribute to the observed experimental spectrum, while the lowest lying Iso-III (D_{2d}) can be ruled out due to its significantly lower collision cross section compared to the experimental value. We would like to clarify this issue in future experiments by performing measurements at reduced nozzle temperatures. Recently, we have extended our experimental spectral tuning range to 4.4 eV which will provide additional information to rationalize our current results in more detail, especially when combined with experiments at lower nozzle temperatures.

The three competing structural motifs and all permutational isomers within these motifs have been rationalized in terms of first order preferences for a particular homotop based on homo- and heterophilicity, electronegativity and atomic radii followed by second order effects such as frustration for charge distributions.

The comparison of the experimental data to optical response calculations shows that the LC-ωPBEh functional describes oscillator strengths for the tetramer cation spectra which are in qualitative agreement with our experimental data. Hence, it is confirmed to be a good xc functional for the description of ground and excited state properties of the cationic tetramer alloys of silver and gold. Therefore, this combined experimental and theoretical approach shows promise as a convenient and efficient procedure for the description of larger mixed Ag-Au cluster cations, which are currently being investigated.

[1] W. A. de Heer, Rev. Mod. Phys. **65**, 611 (1993).
[2] R. Ferrando, J. Jellinek, and R. L. Johnston, Chem. Rev. **108**, 845 (2008).
[3] M. Käll, Nat. Mater. **11**, 570 (2012).
[4] J. K. Gansel, M. Thiel, M. S. Rill, M. Decker, K. Bade, V. Saile, G. von Freymann, S. Linden, and M. Wegener Science **325**, 1513 (2009).
[5] A. W. Castleman Jr., and S. N. Khanna, J. Phys. Chem. C **113**, 2664 (2009).
[6] G. A. Bishea and M. D. Morse, J. Chem. Phys. **95**, 8779 (1991).
[7] S. Fedrigo, W. Harbich, and J. Buttet, J. Chem. Phys. **99**, 5712 (1993).
[8] W. Harbich, S. Fedrigo, and J. Buttet, Z. Phys. D: At., Mol. Clusters **26**, 138 (1993).
[9] B. A. Collings, K. Athanassenas, D. Lacombe, D. M. Rayner, and P. A. Hackett, J. Chem. Phys. **101**, 3506 (1994).
[10] A. Terasaki, S. Minemoto, M. Iseda, and T. Kondow, Eur. Phys. J. D **9**, 163 (1999).
[11] D. Schooss, S. Gilb, J. Kaller, M. M. Kappes, F. Furche, A. Köhn, K. May, and R. Ahlrichs, J. Chem. Phys. **113**, 5361 (2000).
[12] A. Schweizer, J. M. Weber, S. Gilb, H. Schneider, D. Schooss, and M. M. Kappes, J. Chem. Phys. **119**, 3699 (2003).
[13] J. Li, X. Li, H.-J. Zhai, and L.-S. Wang, Science **299**, 864 (2003).
[14] S. Gilb, K. Jacobsen, D. Schooss, F. Furche, R. Ahlrichs, and M. M. Kappes, J. Chem. Phys. **121**, 4619 (2004).
[15] M. Harb, F. Rabilloud, D. Simon, A. Rydlo, S. Lecoultre, F. Conus, V. Rodrigues, and C. Félix, J. Chem. Phys. **129**, 194108 (2008).
[16] P. Gruene, D. M. Rayner, B. Redlich, A. F. G. van der Meer, J. T. Lyon, G. Meijer, and A. Fielicke, Science **321**, 674 (2008).
[17] A. N. Gloess, H. Schneider, J. M. Weber, and M. M. Kappes, J. Chem. Phys. **128**, 114312 (2008).
[18] A. Terasaki, T. Majima, C. Kasai, and T. Kondow, Eur. Phys. J. D **52**, 43 (2009).
[19] K. Egashira, C. Bartels, T. Kondow, and A. Terasaki, Eur. Phys. J. D **63**, 183 (2011).
[20] S. Lecoultre, A. Rydlo, C. Félix, J. Buttet, S. Gilb, and W. Harbich, J. Chem. Phys. **134**, 074302 (2011).
[21] Z. Yang, I. Leon, and L.-S. Wang, J. Chem. Phys. **139**, 021106 (2013).
[22] I. León, Z. Yang, and L.-S. Wang, J. Chem. Phys. **138**, 184304 (2013).
[23] V. Bonačić-Koutecký, V. Veyret, and R. Mitrić, J. Chem. Phys. **115**, 10450 (2001).
[24] J. C. Idrobo, W. Walkosz, S. F. Yip, S. Öğüt, J. Wang, and J. Jellinek, Phys. Rev. B **76**, 205422 (2007).
[25] D. W. Silverstein and L. Jensen, J. Chem. Phys. **132**, 194302 (2010).
[26] S. Goel, K. A. Velizhanin, A. Piryatinski, S. A. Ivanov, and S. Tretiak, J. Chem. Phys. C **116**, 3242 (2012).
[27] J. V. Koppen, M. Hapka, M. M. Szcześniak, and G. Chalasinski, J. Chem. Phys. **137**, 114302 (2012).
[28] Y. Negishi, Y. Nakamura, A. Nakajima, and K. Kaya, J. Chem. Phys. **115**, 3657 (2001).
[29] P. Weis, O. Welz, E. Vollmer, and M. M. Kappes, J. Chem. Phys. **120**, 677 (2004).
[30] V. Bonačić-Koutecký, J. Burda, R. Mitrić, M. Ge, G. Zampella, and P. Fantucci, J. Chem. Phys. **117**, 3120 (2002).
[31] P. Schwerdtfeger, Heteroat. Chem. **13**, 578 (2002).
[32] P. Pyykkö, Annu. Rev. Phys. Chem. **63**, 45 (2012).
[33] G. Jian-Jun, Y. Ji-Xian, and D. Dong, Commun. Theor. Phys. **48**, 348 (2007).
[34] G. F. Zhao and Z. Zeng, J. Chem. Phys. **125**, 014303 (2006).
[35] P. Lu, X.-Y. Kuang, A.-J. Mao, Z.-H. Wang, and Y.-R. Zhao, Mol. Phys. **109**, 2057 (2011).
[36] L. Hong, H. Wang, J. Cheng, X. Huang, L. Sai, and J. Zhao, Comput. Theor. Chem. **993**, 36 (2012).
[37] X.-D. Zhang, M.-L. Guo, D. Wu, P.-X. Liu, Y.-M. Sun, L.-A. Zhang, Y. She, Q.-F. Liu, and F.-Y. Fan, Int. J. Mol. Sci. **12**, 2972 (2011).
[38] G.-F. Zhao, J.-M. Sun, and Z. Zeng, Chem. Phys. **342**, 267 (2007).
[39] R. L. Johnston, Dalton Trans. **2003**, 4193.
[40] S. Heiles, A. J. Logsdail, R. Schäfer, and R. L. Johnston, Nanoscale **4**, 1109 (2012).
[41] S. Heiles, K. Hofmann, R. L. Johnston, and R. Schäfer, ChemPlusChem **77**, 532 (2012).
[42] D. A. Götz, S. Heiles, R. L. Johnston, and R. Schäfer, J. Chem. Phys. **136**, 186101 (2012).
[43] S. Heiles, R. L. Johnston, and R. Schäfer, J. Phys. Chem. A **116**, 7756 (2012).
[44] S. Heiles and R. L. Johnston, Int. J. Quantum Chem. **113**, 2091 (2013).
[45] O. A. Vydrov and G. E. Scuseria, J. Chem. Phys. **125**, 234109 (2006).
[46] O. A. Vydrov, J. Heyd, A. V. Krukau, and G. E. Scuseria, J. Chem. Phys. **125**, 074106 (2006).
[47] M. A. Rohrdanz, K. M. Martins, and J. M. Herbert, J. Chem. Phys. **130**, 054112 (2009).
[48] A. Shayeghi, R. L. Johnston, and R. Schäfer, Phys. Chem. Chem. Phys. **15**, 19715 (2013).
[49] P. Giannozzi, S. Baroni, N. Bonini, M. Calandra, R. Car, C. Cavazzoni, D. Ceresoli, G. L. Chiarotti, M. Cococcioni, I. Dabo, A. Dal Corso, S. de

Gironcoli, S. Fabris, G. Fratesi, R. Gebauer, U. Gerstmann, C. Gougoussis, A. Kokalj, M. Lazzeri, L. Martin-Samos, N. Marzari, F. Mauri, R. Mazzarello, S. Paolini, A. Pasquarello, L. Paulatto, C. Sbraccia, S. Scandolo, G. Sclauzero, A. P. Seitsonen, A. Smogunov, P. Umari, and R. M. Wentzcovitch, J. Phys. Condens. Matter **21**, 395502 (2009).

[50] A. M. Rappe, K. M. Rabe, E. Kaxiras, and J. D. Joannopoulos, Phys. Rev. B **41**, 1227 (1990).

[51] J. Perdew, K. Burke, and M. Ernzerhof, Phys. Rev. Lett. **77**, 3865 (1996).

[52] M. Valiev, E. J. Bylaska, N. Govind, K. Kowalski, T. P. Straatsma, H. J. J. Van Dam, D. Wang, J. Nieplocha, E. Apra, T. L. Windus, and W. A. de Jong, Comput. Phys. Commun. **181**, 1477 (2010).

[53] F. Weigend and R. Ahlrichs, Phys. Chem. Chem. Phys. **7**, 3297 (2005).

[54] F. Rabilloud, J. Phys. Chem. A **117**, 4267 (2013).

[55] W. Tang, E. Sanville, and G. Henkelman, J. Phys. Condens. Matter **21**, 084204 (2009).

[56] Chemissian, *A Computer Program to Analyse and Visualise Quantum-Chemical Calculations* (L. Skripnikov, 2012).

[57] C.-K. Siu, Y. Guo, I. S. Saminathan, A. C. Hopkinson, and K. W. M. Siu, J. Phys. Chem. B **114**, 1204 (2010).

[58] M. F. Mesleh, J. M. Hunter, A. A. Shvartsburg, G. C. Schatz, and M. F. Jarrold, J. Phys. Chem. **100**, 16082 (1996).

[59] Y. Zhao and D. G. Truhlar, J. Chem. Phys. **125**, 194101 (2006).

[60] D. Schooss, P. Weis, O. Hampe, and M. M. Kappes, Philos. Trans. R. Soc. A **368**, 1211 (2010).

[61] A. V. Walker, J. Chem. Phys. **122**, 094310 (2005).

[62] P. Weis, Int. J. Mass Spectrom. **245**, 1 (2005).

[63] C. J. Heard and R. L. Johnston, Eur. Phys. J. D **67**, 34 (2013).

[64] J. Friedrich, S. Gilb, O. T. Ehrler, A. Behrendt, and M. M. Kappes, J. Chem. Phys. **117**, 2635 (2002).

[65] See http://www.bear.bham.ac.uk/bluebear for a description of the Blue-BEAR HPC facility.